ISSN 0030-400X, Optics and Spectroscopy, 2017, Vol. 122, No. 3, pp. 462–468. © Pleiades Publishing, Ltd., 2017.
Original Russian Text © N.Kh. Ibrayev, B.R. Ilyassov, D.A. Afanasyev, 2017, published in Optika i Spektroskopiya, 2017, Vol. 122, No. 3, pp. 475–482.

CONDENSED-MATTER SPECTROSCOPY

Influence of the Morphology of ZnO Nanostructures on Luminescent and Photovoltaic Properties

N. Kh. Ibrayev[a]*, B. R. Ilyassov[a, b], and D. A. Afanasyev[a]

[a] *Institute of Molecular Nanophotonics, Buketov Karaganda State University, Karaganda, 100028 Kazakhstan*
[b] *Laboratory of Solar Energy, PI NLA, Nazarbayev University, Astana 010000, Kazakhstan*
**e-mail: niazibrayev@mail.ru*

Received April 12, 2016; in final form, October 4, 2016

Abstract—Arrays of ZnO nanorods and nanoplates are synthesized by the hydrothermal and electrochemical methods, respectively. The photoluminescence spectra indicate that the nanoplates have a more defective structure than the nanorods. The obtained ZnO nanostructures are used as the basis to construct dye-sensitized solar cells. The influence of morphology and defectiveness of ZnO nanostructures on the luminescent and photovoltaic properties of the cells is studied.

DOI: 10.1134/S0030400X17030092

INTRODUCTION

ZnO, a wide bandgap semiconductor with the energy of ~3.3 eV of the forbidden zone at 300 K, is of interest for use in various optoelectronic devices, including the new generation of organic-inorganic solar cells (the organic-inorganic perovskite cells [1–3] and dye-sensitized solar cells (DSSCs) [4, 5]).

Depending on the methods of synthesis, ZnO nanostructures can be obtained with different morphologies and properties. ZnO nanostructures of various morphologies are used in DSSCs, including nanoporous films [6], nanorods [4, 5], nanoplates [5], tetrapods, and various hierarchical nanostructures [7]. Nonetheless, the energy conversion efficiency in ZnO-based DSSCs is usually significantly lower than in cells based on TiO_2 [8]. To date, the maximum achieved efficiency of DSSCs based on ultrathin ZnO nanorods is 7% [9], which remains significantly lower than that of TiO_2 cells. The typical value of the efficiency reported in many studies is of the order of 1% or lower [10]. The low efficiency of the ZnO cells compared to the TiO_2 cells, despite the similarity of their band structure [8], can be partly attributed to the decomposition of ZnO and the formation of dye/Zn^{2+} aggregates [8, 11], the low efficiency of the injection of the electron from the dye to ZnO [8, 11], the low efficiency of the recovery of the dye [8], and the high density of surface defects (electron capture centers) [12]. Nonetheless, in contrast to TiO_2, ZnO has a large variety of nanocrystals of different morphologies with a high specific surface, which can be obtained by the methods of synthesis from solutions at temperatures below 100°C [13–16]. In addition, the mobility of electrons, at least in ZnO single crystals is an order of magnitude higher than in TiO_2 (anatase structure) [17–20]. For this reason, there is significant interest in improving the manufacturing technology and electron transport properties of DSSCs with the use of nanostructured ZnO electrodes with different morphologies.

A significant amount of work on modification of the ZnO morphology has been performed with the aim of improving the efficiency of DSSCs [6, 17, 21]. In particular, these studies were aimed at increasing the specific surface area and, simultaneously, improving the accumulation of charge which provides faster transport of electrons. The increase in the efficiency of the cells upon modification of the morphology is due to the faster transport of electrons [22, 23], the increase in the amount of adsorbed dye [22, 23], and the increase in the electron lifetime [24]. There are other possible ways of improving the efficiency of DSSCs, including, for example, the use of surface plasmon resonance [25, 26]. However, the dependence of the cell efficiency on these factors is likely more complicated. It has been shown that a higher efficiency can be obtained for a shorter electron lifetime if the electron transport is shorter or if the efficiencies of the electron injection and the dye recovery are higher [8]. Although the optimization of the morphology increases the efficiency of DSSCs based on ZnO, it is obvious that the efficiency is also determined by the ZnO properties (the types of defects and their concentration and charge transfer in ZnO). Despite the importance of the ZnO properties for the performance of solar cells based on ZnO, there are very few studies on the relationship between the prop-

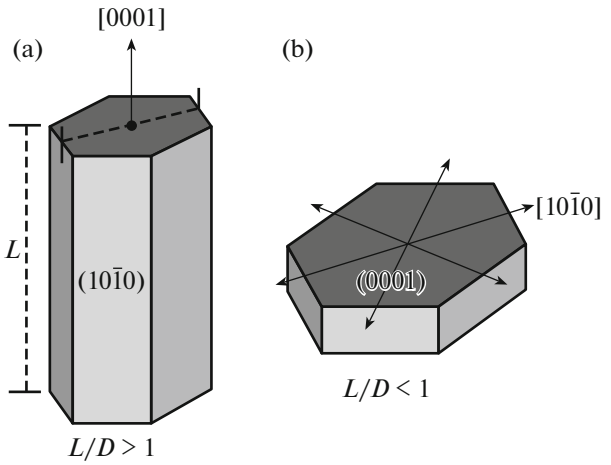

Fig. 1. Schematic representation of (a) a nanorod and (b) a nanoplate.

erties of ZnO nanostructures and solar cells based on them [27, 28].

In this work we study two different ZnO nanostructures: nanorods and nanoplates and the influence of their morphology on the luminescent and photovoltaic properties. The ZnO nanorods and nanoplates were synthesized respectively by the methods of hydrothermal and electrochemical deposition. The ZnO nanorods and nanoplates are nanocrystals with different ratios of geometrical characteristics (the L/D ratio, see Fig. 1). The nanorods are formed when the preferential direction of the crystal growth is [0001], which leads to a morphology with a large value of the L/D ratio and a large area of the $(10\bar{1}0)$ faces. The nanoplates are formed when the preferential direction of the crystal growth is $[10\bar{1}0]$, which leads to the morphology with a low value of L/D and a large area of the $(0001)/(000\bar{1})$ faces.

The ZnO nanorods and nanoplates exhibit significantly different optical properties, adsorption of the dye, and photovoltaic properties. The nanorods have a higher intensity of the edge photoluminescence in the UV region compared to the intensity in the visible region of the spectrum (this points to a low concentration of defects). The nanoplates have the opposite photoluminescent properties: the intensity of the luminescence bands in the visible region is much higher than the intensity of the edge photoluminescence band (this indicates a high concentration of defects). The temporal characteristics of the edge photoluminescence of ZnO were also measured. The character of photoluminescence of the ZnO nanostructures influences their photovoltaic properties. The presence of defects responsible for green-yellow emission leads to a decrease in the open-circuit voltage (U_{OC}) of DSSCs.

EXPERIMENTAL

Synthesis of arrays of ZnO nanorods. The synthesis of ZnO nanorods consisted of two stages. The first stage is the application of a seed layer and the second stage is the synthesis of nanorods on the substrate with the seed layer by hydrothermal deposition.

Application of the seed layer of ZnO. Zinc acetate dihydrate ($Zn(CH_3COO)_2 \cdot 2H_2O$, SigmaAldrich) and monoethanolamine (C_2H_7NO, Sigma Aldrich) were sequentially dissolved in isopropyl alcohol. The concentrations of zinc acetate and monoethanolamine in the prepared solution were 0.5 M. The solution was applied on a precleaned glass substrate covered with a conductive layer of indium-doped tin oxide (ITO). This procedure was repeated 4 times by the spin-coating method with a substrate rotation speed of 2000 rpm. Next, for forming the ZnO structures, the substrate was annealed in a muffle furnace at a temperature of 450°C for 60 min.

Hydrothermal deposition. The arrays of ZnO nanorods were synthesized on ITO-substrates with a preapplied seed ZnO layer from an equimolar aqueous solution of zinc nitrate ($Zn(NO_3)$, Sigma Aldrich) and hexamine ($C_6H_{12}N_4$, Sigma Aldrich) for 10 h. The initial concentration of the solution and the temperature of synthesis were 25 mM and 90°C. After each 2 h, the samples were washed in deionized water and placed in a fresh solution. After completion of the synthesis, the grown ZnO arrays were repeatedly washed in deionized water, dried, and annealed at a temperature of 400°C for 1 h.

Synthesis of arrays of ZnO nanoplates. Arrays of ZnO nanoplates were obtained according to the method described in [29]. The first step was the synthesis of an array of hexagonal $Zn_5(OH)_8C_{l2}$ plates on an ITO substrate by electrochemical deposition from a solution of 5 mM $ZnNO_3$ (Sigma-Aldrich) and 100 mM KCl. Electrochemical deposition was carried out using a J-30 potentiostat–galvanostat (Elins) in the potentiostat mode at a potential of –1050 mV (relative to the silver chloride electrode) and a solution temperature of 50°C for 30 min. Then, the precipitated arrays of the $Zn_5(OH)_8C_{l2}$ nanoplates were annealed at a temperature of 450°C for 30 min to form ZnO nanorodes.

Assembling a DSSC. Ruthenium dye N719 (Ditetrabutylammonium cis-bis(isothiocyanato)bis(2,2'-bipyridyl-4,4'-dicarboxylato)ruthenium(II), Sigma Aldrich) was used to assemble DSSCs. The dye was dissolved in absolute ethanol (concentration 0.3 mM). The resulting arrays of ZnO nanorods and nanoplates were immersed in an alcoholic solution of the dye for 30 minutes at a temperature of 60°C, rinsed in ethanol, and dried. The assembled cell had a sandwich structure, consisting of a sensitized photoanode and an contra-electrode with a platinum coating. The electrodes were separated by a polymer spacer with a

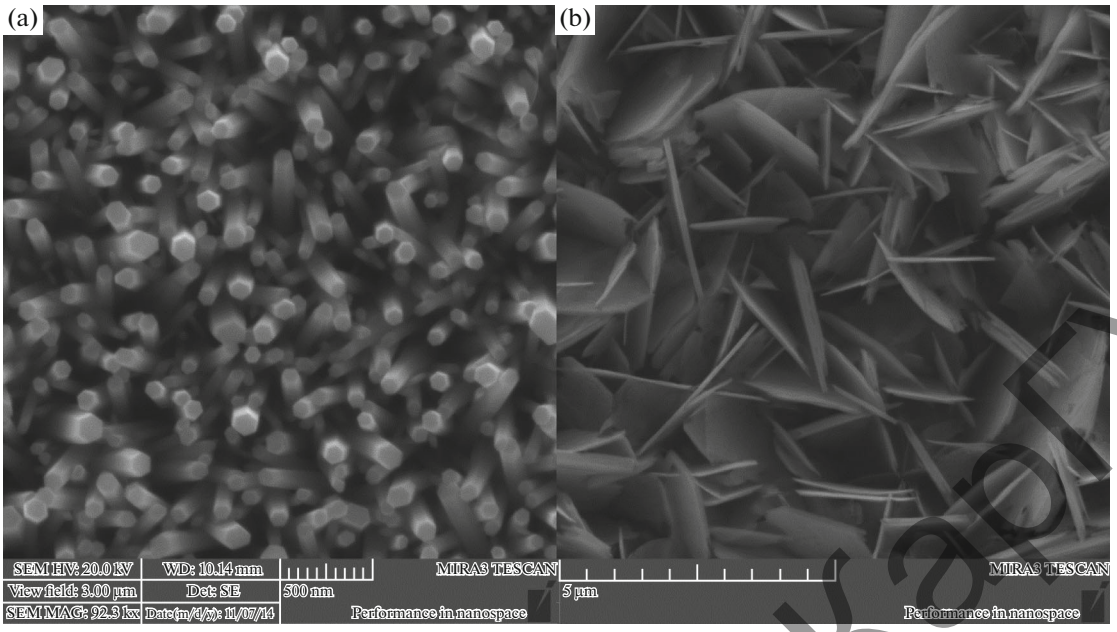

Fig. 2. Array of ZnO nanorods (a) and nanoplates (b).

0.2 cm^2 hole, which defines the active area of the cell. The platinum coating was deposited by the electrochemical method onto glass substrates with a conductive ITO layer. An Iodolyte Z-150 electrolyte (Solaronix) was introduced into the active area of the cell through a small hole in the contra-electrode.

Measurements. The morphology of the obtained samples was investigated using a Mira-3 scanning electron microscope with a Schottky cathode (Tescan). The spectra of X-ray diffraction were measured on a DRON-7 electron diffractometer. The current-voltage characteristics (CVCs) of the cells were measured using a Keithley 2400 source measure unit under exposure to the emission of an AM 1.5 100 mW/cm^2 standard solar radiation simulator (PET PHOTO Emission Tech., Inc.). Luminescence spectra were measured on an AvaSpec-2048 high-sensitivity fiber optic spectrometer at room temperature. Photoexcitation of the samples was carried out with the third harmonic of a LCS-DTL-374QT neodymium laser ($\lambda = 355$ nm, $\tau = 7$ ns, $E = 5$ μJ). The temporal characteristics of short-lived luminescence were measured using a pulsed spectrofluorimeter (Becker&Hickl), which was operated in the time correlated single photon counting mode. The samples were excited by picosecond semiconductor laser (BDL-SMC) emitting at $\lambda = 375$ nm with a repetition frequency of 50 MHz and a pulse duration of 50 ps. The kinetics of luminescence with a slow decay rate were measured with a setup operating in the photon counting mode [30]. Photoexcitation of the samples was carried out with the third harmonic of a LCS-DTL-374QT neodymium laser. The registration system consisted of PMT with an H7421 electronic unlocking system, a C8744 discriminator, and a M8784 pulse counter (Hamamatsu Photonics).

RESULTS AND DISCUSSION

Figure 2 shows the SEM images of the arrays of ZnO nanorods and nanoplates obtained by hydrothermal and electrochemical deposition, respectively. As is seen from Fig. 2a, the nanorods have a hexagonal shape, mostly vertical orientation perpendicular to the substrate, and practically the same length, diameter, and distribution density. The average diameter and length of the nanorods for the given synthesis conditions are 150 nm and 3.3 μm, respectively. The nanoplates (Fig. 2b) also have a hexagonal shape with a diameter of 4–5 μm and a thickness of about 100 nm. Unlike nanorods, with their hexagonal plane being predominantly parallel to the substrate, the nanoplates are mainly oriented perpendicular to the substrate.

Figure 3 shows the X-ray spectra of the obtained nanostructures. All diffraction peaks are assigned according to the wurtzite structure of ZnO (spatial group $p63mc$). In contrast to the nanoplates, the X-ray spectra of the nanorods (Fig. 3a) display an intense peak at $2\theta \sim 34^o$, which indicates that the nanorods are preferably oriented along the direction of the crystallographic c axis perpendicular to the substrate. According to the SEM and X-ray data, the L/D ratio of the sides (see Fig. 1) for the nanorods is ~22 and $\sim 24 \times 10^{-3}$ for the nanoplates; i.e., the difference is three orders of magnitude.

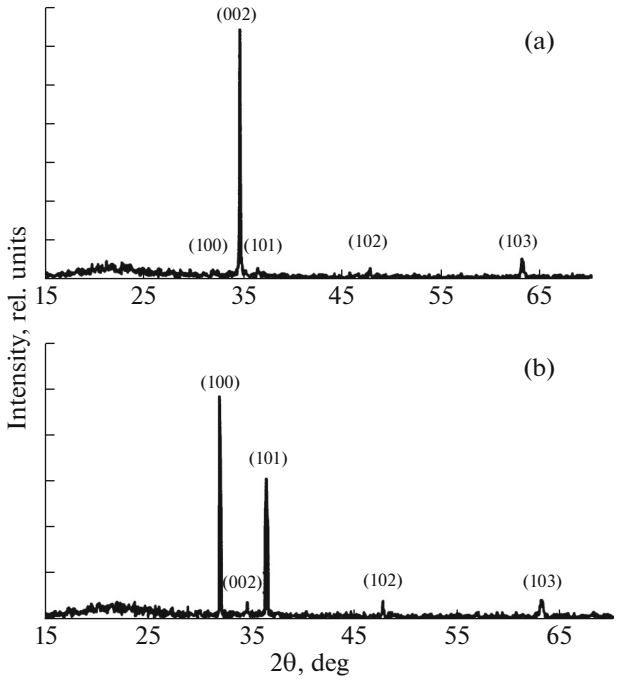

Fig. 3. X-ray diffraction spectra of (a) ZnO nanorods and (b) nanoplates.

The luminescence spectra of the ZnO nanorods and nanoplates are shown in Fig. 4. As can be seen, the luminescence spectra consist of two bands: a narrow band in the UV region with a maximum at 380 nm and a broad band in the visible region. In the spectrum of nanorods, the band in the visible region clearly exhibits two peaks at 546 and 576 nm, respectively. The spectrum of nanorods in the visible region is very weak. However, similar peaks at 546 and 576 nm can be distinguished. The UV band has an excitonic nature, with the free and bound excitons being the main emission sources [31]. The luminescence of the ZnO nanostructures in the visible region is associated with the defects, the nature of which remains controversial [31, 32]. As shown in [33], the green luminescence of the ZnO nanostructures is due to surface defects. Moreover, in a number of works [34, 35], where a similar green-yellow luminescence was observed as in the present study, interstitial zinc (Zn_i) is assigned to a native shallow donor in ZnO, while oxygen vacancies are assigned to the deep donors. The last assumption has been supported by the theoretical calculations [36].

As follows from the luminescence spectra, the defectiveness of the ZnO nanoplates is much more significant in comparison with the nanorods. The ratio of the maximum intensity of the luminescence band in the visible region, I_{VR}, to the maximum intensity of the edge luminescence band (ELB) in the shortwavelength region, I_{UV} [35], is frequently used to determine the crystallinity of the ZnO nanostructures. The I_{VR}/I_{UV} ratio for the nanorods is much less than unity indicating their good crystallinity, while for the nanorods I_{VR}/I_{UV} is much larger than unity indicating a significant defectiveness of the structure.

Figure 5 shows the kinetics of the ELB decay for the nanorods and nanoplates. The ELB of ZnO decays in the subnanosecond range [31]. As can be seen from Figs. 4, 5, and 6, the decay kinetics of ELB for both the nanorods and nanoplates is a nonexponential function. Each kinetic curve of the ELB decay can be divided into two exponential parts (Fig. 6). The lifetimes calculated from these curves are ~1.1 and 2.33 ns for the nanorods and 0.71 and 1.7 ns for the nanoplates. As can be seen, the ELB of nanoplates decays faster than that of the nanorods.

The significant differences of the luminescent properties of ZnO nanorods and nanoplates can be associated with a significant difference in the morphologies of these nanostructures. As mentioned earlier, the contribution of the $(0001)/(000\bar{1})$ faces of the ZnO crystal in the total surface of the array of the nanoplates is huge. Perhaps most of the surface defects

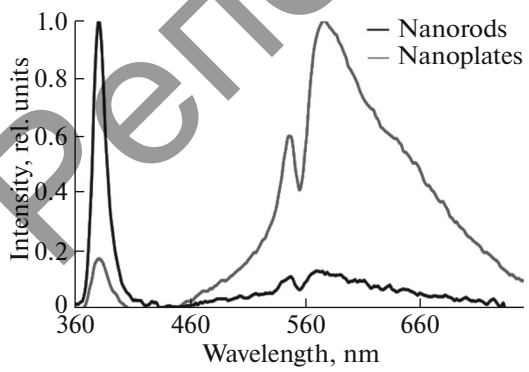

Fig. 4. Luminescence spectra of ZnO nanorods and nanoplates.

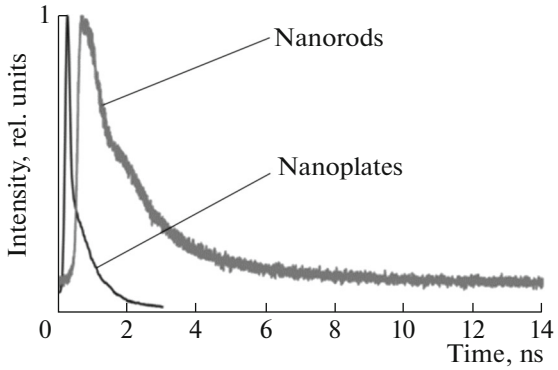

Fig. 5. Decay kinetics of the edge luminescence band (ELB) of the ZnO nanorods and nanoplates.

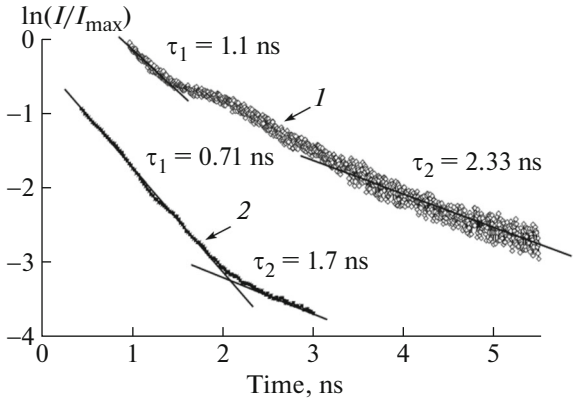

Fig. 6. Decay kinetics of (ELB) of the (*1*) ZnO nanorods and (*2*) nanoplates (the lifetime was determined by linear approximation).

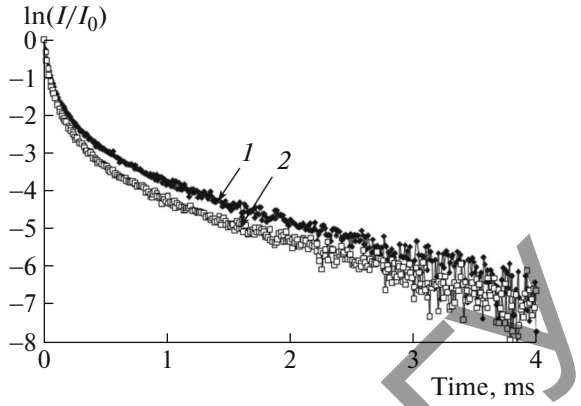

Fig. 7. Kinetics of the long-wave luminescence of (*1*) ZnO nanorods and (*2*) nanoplates.

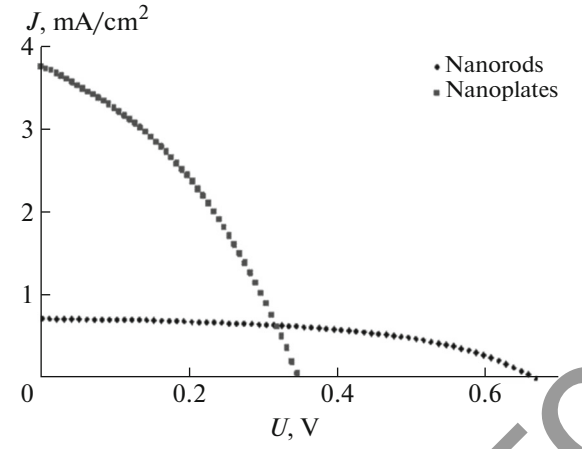

Fig. 8. Volt-ampere characteristics of DSS cells based on ZnO nanorods and nanoplates.

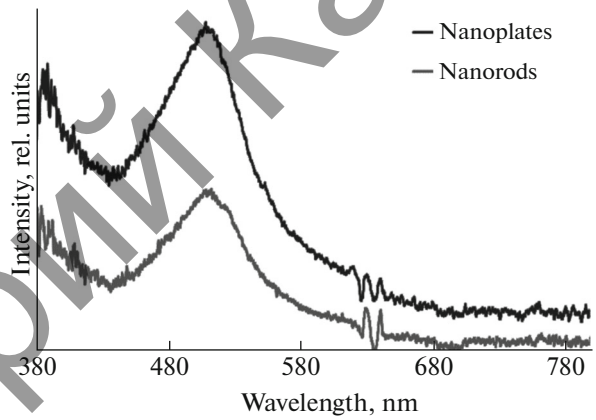

Fig. 9. Optical density of a dye solution desorbed from nanorods and nanoplates.

in ZnO is concentrated on these faces. However, more detailed studies are necessary for confirmation.

The decay kinetics of the long wavelength luminescence of the ZnO nanostructures is shown in Fig. 7. For both nanostructures the decay curves have almost the same shape. The lifetimes calculated from the linear part of the curves are of 1 ms. It should be noted that the luminescence duration remains the same in the temperature range from the room temperature to the boiling temperature of liquid nitrogen. The identical lifetime of the slow luminescence (SL) indicates that the defects in the nanorods and nanoplates are of the same nature. Because KCl was used only in the electrochemical synthesis of the nanoplates, K and Cl can be excluded from the list of elements, leading to the formation of the impurity centers responsible for the SL of ZnO. Comparing the present results for spectral dependence and lifetimes of the SL to the results given in [37], one can assume that the formation of SL involves oxygen and zinc vacancies.

The synthesized ZnO nanostructures were used to make DSSCs for studying their photovoltaic properties. The volt-ampere characteristics and photovoltaic parameters of DSSCs based on the studied ZnO nanostructures are shown in Fig. 8 and the table.

As can be seen from the table, the efficiency of cells (η) based on nanoplates is twice that of cell based on nanorods. This is because the density of the short-circuit current (J_{sc}) of DSSCs based on nanoplates (NP DSSCs) is 5–6 times higher than that of DSSCs based on ZnO nanorods (NR DSSCs). However, the open-circuit voltage (U_{oc}) of NP DSSCs is almost half that of NR DSSCs and the fill factor (FF) of NP DSSCs is significantly lower than the FF of NR DSSCs.

Since the same dye was used in both cases, the difference in J_{sc} most likely is due to a larger specific surface of the nanoplates. Figure 9 shows the spectra of the optical density of the dye in a solution of water/isopropyl alcohol (50/50) desorbed from the nanorods

Photovoltaic properties of DSS cells based on ZnO nanorods and nanoplates

Cell type	J_{sc}, mA/cm^2	U_{oc}, V	FF	η, %
Nanorod-based DSSC	0.68	0.66	0.52	0.25
Nanoplate-based DSSC	3.72	0.37	0.36	0.50

and nanoplates. As can be seen from Fig. 9, the solution of the dye desorbed from the nanoplates has a higher optical density compared to the dye desorbed from the nanorods, which indirectly indicates that the nanoplates adsorb more dye molecules and, thus, have a larger specific surface than the nanorods under the given synthesis conditions.

However, it is possible that photoinjection of electrons from the dye molecules to ZnO occurs more efficiently through the ZnO (0001) plane, which, in contrast to the nanorods, makes a dominant contribution to the surface area of the ZnO nanoplates.

The density of the point defects in a semiconductor has a significant impact on the DSSC photo-voltage. The defects can act as capture centers of the photoinjected electrons and, thus, decrease their concentration in the conduction band. The cell photovoltage is determined by the difference between the Fermi quasi-level of the semiconductor (ZnO) under exposure to light and the electrochemical potential of the electrolyte [38]. The position of the Fermi quasi-level in the semiconductor depends on the concentration of the electrons in the conduction band (n). The greater the concentration of electrons injected from the dye molecules to the conduction band under the action of light, the closer the Fermi quasi-level to the bottom of the conductivity zone, which increases U_{oc}. The open circuit voltage of the DSSCs is given by [39]:

$$V_{OC} = \frac{E_{F_n} - E_{F_0}}{e} = \frac{k_B T}{e} \ln\left(\frac{n}{n_0}\right),$$

where $k_B T$ is the thermal energy, e is the elementary charge, and n_0 is the dark concentration of electrons in the conduction band. It is obvious that the electron capture by traps has a significant effect on the U_{oc} generated upon permanent exposure to light. Therefore, the low value of U_{oc} of NP DSSCs may be due to the influence of the defects responsible for the ZnO luminescence in the visible region.

CONCLUSIONS

Thus, in this work we studied the luminescent and photovoltaic properties of ZnO nanorods and nanoplates synthesized by hydrothermal and electrochemical deposition, respectively. The nanorods are characterized by a higher intensity of the edge luminescence band in the short wavelength region of the spectrum in comparison with the intensity of photoluminescence in the visible (green-yellow region) which indicates their good crystallinity. The nanoplates exhibit the opposite photoluminescent properties: the intensity of the luminescence bands in the visible region is much higher than the intensity of the edge luminescence band indicating a high concentration of defects in the nanoplates. The short-circuit current of the DSSCs based on ZnO nanoplates is 5–6 times greater than that of the cells based on nanorods, which is likely due to the greater specific surface of the nanoplates. This is confirmed by the measurements of dye photoabsorption. The open-circuit photovoltage of DSSCs based on ZnO nanorods is almost double that of the cells based on ZnO nanoplates. The smaller photovoltage of DSSCs based on nanoplates can be due to the defects responsible for the luminescence of the ZnO nanoplates in the visible region; these defects can act as capture centers of the photoinjected electrons and lower the Fermi quasi-level of electrons in ZnO. The obtained data show a good correlation between the luminescent and photovoltaic properties of zinc oxide nanostructures.

ACKNOWLEDGMENTS

This work was supported by the Ministry of Education and Science of the Republic of Kazakhstan (grant 0088/PAF-15 and grant 1122/GF4) and N0115RK03029 “NU-Berkley strategic initiative in warm-dense matter, advanced materials and energy sources for 2014–2018” from the Ministry of Education and Science of the Republic of Kazakhstan.

REFERENCES

1. D.-Y. Son, J.-H. Im, H.-S. Kim, and N.-G. Park, J. Phys. Chem. C **118**, 16567 (2014). doi 10.1021/jp412407j
2. M. H. Kumar, N. Yantara, S. Dharani, et al., J. Chem. Commun. **49**, 11089 (2013). doi 10.1039/c3cc46534a
3. D. Liu and T. L. Kelly, Nat. Photon. **8**, 133 (2014). doi 10.1038/nphoton.2013.342
4. B. R. Ilyassov, N. Kh. Ibraev, and D. B. Abzhanova, IOP Conf. Ser.: Mater. Sci. Eng. **81**, 012046 (2015). doi 10.1088/1757-899X/81/1/012046
5. B. Ilyassov, N. Ibrayev, and N. Nuraje, Mater. Sci. Semicond. Process. **40**, 885 (2015). doi 10.1016/j.mssp.2015.07.087
6. V. M. Guerin, C. Magne, T. Pauporté, T. le Bahers, and J. Rathousky, J. ACS Appl. Mater. Interfaces **2**, 3677 (2010). doi 10.1021/am1008248
7. R. R. Bacsa, J. Dexpert-Ghys, M. Verelst, et al., J. Adv. Funct. Mater. **19**, 875 (2009). doi 10.1002/adfm.200801049
8. M. Quintana, T. Edvinsson, A. Hagfeldt, and G. Boschloo, J. Phys. Chem. C **111**, 1035 (2007).
9. Xu Chengkun, Wu Jiamin, Desai V. Umang, and Gao Di, J. Am. Chem. Soc. **133**, 8122 (2011). doi 10.1021/ja202135n
10. R. Marczak, F. Werner, R. Ahmad, et al., Langmuir **27**, 3920 (2011). doi 10.1021/jp065948f

11. H. Horiuchi, R. Katoh, K. Hara, et al., J. Phys. Chem. B **107**, 2570 (2003). doi 10.1021/jp0220027
12. J. J. Wu, G. R. Chen, H. H. Yang, C. H. Ku, and J. Y. Lai, Appl. Phys. Lett. **90**, 213109 (2007). doi 10.1063/1.2742639
13. S. Baruah and J. Dutta, J. Sci. Technol. Adv. Mater. **10**, 013001 (2009). doi 10.1088/1468-6996/10/1/013001
14. Z. Lamia, J. Mater. Sci. Eng. B **174**, 18 (2010). doi 10.1016/j.mseb.2010.07.001
15. M. Skompska and K. Zarebska, J. Electrochim. Acta **127**, 467 (2014). doi 10.1016/j.electacta.2014.02.049
16. H. Chen, L. Zhu, H. Liu, and W. Li, J. Thin Solid Films **534**, 205 (2013). doi 10.1016/j.tsf.2013.02.060
17. M. Law, L. E. Greene, and P. Yang, Nat. Mater. **4**, 455 (2005). doi 10.1038/nmat3069
18. Y. Gao, M. Nagai, T.-C. Chang, and J.-J. Shyue, J. Cryst. Growth Des. **7**, 2467 (2007). doi 10.1021/cg060934k
19. E. M. Kaidashev, M. Lorenz, H. von Wenckstern, et al., Appl. Phys. Lett. **82**, 3901 (2003). doi 10.1063/1.1578694
20. E. Hendry, M. Koeberg, B. O'Regan, and M. Bonn, J. Nano Lett. **6**, 755 (2006). doi 10.1021/nl0600225
21. C. T. Wu, W. P. Liao, and J. J. Wu, J. Mater. Chem. **21**, 2871 (2011). doi 10.1021/nl0600225
22. H. P. Dong, L. D. Wang, R. Gao, Y. J. Qiu, and B. B. Ma, J. Mater. Chem. **21**, 19389 (2011). doi 10.1039/ C1JM14191K
23. C. T. Wu and J. J. Wu, J. Mater. Chem. **21**, 13605 (2011). doi 10.1039/C1JM11681A
24. Y. H. Lai, C. Y. Lin, H. W. Chen, et al., J. Mater. Chem. **20**, 9379 (2010). doi 10.1039/C0JM01787F
25. C. K. Peh, L. Ke, and G. W. Ho, Mater. Lett. **64**, 1372 (2010). doi 10.1016/j.matlet.2010.03.022
26. N. Kh. Ibrayev, A. K. Aimukhanov, and A. K. Zeinidenov, IOP Conf. Ser.: Mater. Sci. Eng. **110**, 012067S (2016). doi 10.1088/1757-899X/110/1/012067
27. Y. F. Hsu, Y. Y. Xi, A. B. Djurišić, and W. K. Chan, Appl. Phys. Lett. **92**, 133507 (2008). doi 10.1063/1.2906370
28. H. M. Gao, G. J. Fang, M. J. Wang, et al., J. Mater. Res. Bull. **43**, 3345 (2008). doi 10.1016/j.materresbull.2008.02.010
29. F. Xu, M. Dai, Y. Lu, and L. Sun, J. Phys. Chem. C **114**, 2776 (2010). doi 10.1021/jp910363w
30. D. A. Afanasyev and R. J. Gimazetdinov, Bull. Univ. Karaganda, Ser. Phys., No. 2 (50), 71 (2008).
31. P. A. Rodnyi and I. V. Khodyuk, Opt. Spectrosc. **111**, 814 (2011). doi 10.1134/S0030400X11120216
32. A. B. Djurišić, Y. H. Leung, K. H. Tam, et al., Appl. Phys. Lett. **88**, 103107 (2006). doi 10.1063/1.2182096
33. D. Li, Y. H. Leung, A. B. Djurišić, Z. T. Liu, et al., Appl. Phys. Lett. **85**, 1601 (2004). doi 10.1063/1.1786375
34. F. Morazzoni, R. Scotti, P. Di Nola, C. Milani, and D. Narducci, J. Chem. Soc., Faraday Trans. **88**, 1691 (1992). doi 10.1039/FT9928801691
35. D. Li et al., Appl. Phys. Lett. **85**, 1601 (2004). doi 10.1063/1.1786375
36. H. Chen et al., J. Lumin. **131**, 1189 (2011). doi 10.1016/j.jlumin.2011.02.025
37. G.-Q. Tang, Y. Xiong, L. Z. Zhang, and G.-L. Zhang, Chem. Phys. Lett. **395**, 97 (2004). doi 10.1016/j.cplett.2004.07.067
38. B. O' Regan and M. Gräzel, Nature **353**, 373 (1991). doi doi 10.1038/353737a0
39. J. Bisquert, A. Zaban, and P. Salvador, J. Phys. Chem. B **106**, 8774 (2002). doi 10.1021/jp011941g

Translated by V. Alekseev